



Extension induced phase separation and crystallization in semidilute solutions of ultra high molecular weight polyethylene

Sara Lindeblad Wingstrand ^a, Luna Imperiali ^b, Roman Stepanyan ^b, Ole Hassager ^{a,*}

^a Technical University of Denmark, Department of Chemical and Biochemical Engineering, Danish Polymer Center, DK-2800, Kgs. Lyngby, Denmark

^b DSM Research Performance Materials, Materials Science Center, NL-6160BB Geleen, The Netherlands

ARTICLE INFO

Article history:

Received 8 September 2017

Received in revised form

7 December 2017

Accepted 17 December 2017

Available online 21 December 2017

Keywords:

Crystallization

Extensional flow

Rheology

ABSTRACT

We investigate the influence of controlled uniaxial extension on various flow induced phenomena in semidilute solutions of ultra high molecular weight polyethylene. Concentrations range from 9 w% to 29 w% and the choice of solvent is paraffin oil. The start-up extensional behavior is measured at various Hencky strain rates $\dot{\epsilon}$ and at two different temperatures (150 °C and 170 °C) well above the melting point. For Hencky strains $\epsilon > 0.9$ the qualitative behavior of the samples differ significantly depending on the imposed conditions and the concentration of the samples. Overall we propose two flow scenarios: Scenario 1 - flow induced phase separation resulting in an unstable bulky filament and Scenario 2 - flow induced phase separation and crystallization resulting in a stable deformation and a smooth strongly strain hardening filament. Scenario 2 is observed only at 150 °C at high $\dot{\epsilon}$ and high concentrations. Scenario 1, observed at both temperatures, is most pronounced at low rates and/or high concentrations.

© 2017 Elsevier Ltd. All rights reserved.

1. Introduction

Ultra high modulus polyethylene fibers are spun from solutions of ultra high molecular weight polyethylene (UHMwPE) [1]. To a large extent fiber spinning processes comprise uniaxial extensional upon extrusion and drawing of the polymeric liquid. The processability of UHMwPE solutions is thus determined by the rheological characteristics primarily in extension, yet controlled rheological studies of PE solutions have been performed only in shear flow [2].

In shear, UHMwPE solutions exhibit significant nonlinear characteristics [3]. The long chains are easily deformed by flow causing the solutions to be highly shear thinning. Several studies on UHMwPE solutions utilize paraffin oil (PO) as solvent. It is a convenient solvent due to its low volatility and the fact that the chemical composition is the same as that of UHMwPE. Extensive work on UHMwPE/PO solutions in shear have been performed by Murase and co-workers [4–7]. Apart from significant shear thinning they discovered other highly nonlinear phenomena in these systems. They found that multiple states of heterogeneities can be initiated by flow under the right conditions. At high shear rates the UHMwPE/PO solutions experience concentration fluctuations that

eventually develop into actual phase separation [4]. In addition, at temperatures close to the melting point T_m , the UHMwPE rich phase crystallizes into highly oriented structures [5,6]. These flow induced phenomena have been found to play a huge role in the structural development of UHMwPE fibers during processing [7] as well as the final fiber strength [8,9]. Unfortunately, the deformation in a spin-line is ill defined and lacks control of the deformation. As a result, the imposed deformation is quantified in terms of take-up speed or other measures related to the instrument rather than local deformation of the material. Due to experimental challenges regarding both control of the deformation and the non-stick nature of the sample, studies on polyethylene solutions in controlled extensional flows have, to our knowledge, never been performed.

The purpose of the present study is to characterize solutions of UHMwPE in controlled uniaxial extension. The solvent is PO and the samples are measured at constant deformation rates at temperatures well above T_m . Extension of these non-sticky samples are performed using a filament stretch rheometer (FSR) with a modified sample plate design to prevent slip off. Conditions under which flow induced phase separation and flow induced crystallization (FIC) occur are identified using simultaneous high-speed imaging. We map the regimes under which the different flow induced phenomena occur with respect to imposed deformation rate, polymer concentration, and temperature.

* Corresponding author.

E-mail address: oh@kt.dtu.dk (O. Hassager).

2. Materials and method

UHMWPE with $M_w = 3\,500\,000\text{ g/mol}$ and a broad molar mass distribution, supplied by DSM and paraffin oil (containing 0.2 w% antioxidant: 2,6-di-tert-butyl-p-cresol) were mixed in an extruder at a temperature well above the melting temperature. Three solutions were prepared containing 5 w%, 10 w% and 20 w% UHMWPE. The solutions were extruded directly into a mould and moulded into discs of diameter $D_0 = 8\text{ mm}$ and height $h_0 = 6\text{ mm}$.

Upon cooling to room temperature, some solvent was expelled from the sample due to crystallization of the UHMWPE. Hence, before starting rheological characterizations, the concentration of polymer in the remaining gel samples was determined using TGA (Discovery TGA from TA Instruments). Concentrations were determined from the integrals under the clearly separated PO and UHMWPE peaks (see Supplemental Material for details). The melting point was determined by DSC with an auto sampler from TA instruments (Discovery DSC from TA instruments). In Table 1 specifications regarding polymer concentration obtained from TGA and nominal melting temperature T_m obtained from DSC are given. Table 1 also presents the average number of entanglements Z and the Flory-Huggins predicted equilibrium melting point. The number of entanglements is given by $Z = (M_w/M_e)\phi^\alpha$ where the molar mass between entanglements $M_e = 1120\text{ g/mol}$ [10] (Note here we assume a dilution exponent $\alpha = 1$). T_m predicted by Flory-Huggins is given by [11].

$$\frac{1}{T_m} - \frac{1}{T_m^0} \cong \frac{R}{\Delta H_f} \left[(1 - \phi) - \chi(1 - \phi^2) \right] \quad (1)$$

The equilibrium melting point of the bulk polymer T_m^0 is set to $145\text{ }^\circ\text{C}$ and $\Delta H_f = 3900\text{ kJ/mol}$ is the heat of fusion [5]. The interaction parameter χ is set to 0 as the chemical composition of PE and PO is the same.

Melting temperatures measured by DSC are higher than predicted by Eq. (1). This difference is expected as melting of the PE crystals during the DSC heating ramp does not take place instantaneously. Kinetic delay pushes the melting to higher temperatures in the DSC and thus it tends to overestimate the T_m .

2.1. Small angle oscillatory shear (SAOS)

The linear rheology of the solutions was measured in SAOS. An ARES G2 rheometer from TA Instruments was used with a 25 mm plate-plate geometry. To prevent degradation of the sample, measurements were carried out in the presence of nitrogen. The samples were heated to $170\text{ }^\circ\text{C}$ and left to relax. Frequency spectra were collected for $T = 150\text{ }^\circ\text{C}$ and $170\text{ }^\circ\text{C}$. At higher temperatures the loss of solvent was so significant that the rheology no longer was reproducible. Frequency sweeps obtained at different temperatures were shifted and combined into one master curve for each sample.

Table 1
Material characteristics of the prepared solutions of UHMWPE in paraffin oil.

| Sample | ϕ [w%] | T_m [$^\circ\text{C}$] ^a | T_m [$^\circ\text{C}$] ^b | Z |
|-----------|-------------|---|---|-----|
| PE/PO-29% | 28.7 | 123.5 | 119.2 | 960 |
| PE/PO-17% | 16.8 | 121.6 | 115.8 | 560 |
| PE/PO-9% | 8.8 | 118.9 | 113.6 | 293 |

^a From DSC.

^b From Eq. (1).

2.2. Combined filament stretch rheometry and high-speed imaging of non-sticky samples

Extensional rheometry was carried out on a VADER 1000 filament stretch rheometer (FSR) from Rheofilament. The advantage of the FSR is that it allows for controlled deformation to large Hencky strains $\varepsilon > 7$ via a feed back loop [12].

The FSR comprises a moving top plate and a stationary bottom plate between which the sample is sandwiched. Upon movement of the top plate, the fluid is extended uniaxially due to the no slip boundary condition on the plates [13]. The deformation is measured in the mid-filament plane using a laser micrometer and the response of the fluid is monitored via a force cell mounted on the bottom plate. The measure for deformation and response of the fluid is Hencky strain ε and first normal stress difference $\sigma_{zz} - \sigma_{rr}$, respectively:

$$\varepsilon = -2 \ln \frac{D(t)}{D_0} \quad (2)$$

$$\sigma_{zz} - \sigma_{rr} = \frac{F(t) - \frac{1}{2}m_f g}{\frac{\pi}{4}D(t)^2} \quad (3)$$

Here $D(t)$ and D_0 are the measured and initial diameter, respectively. $F(t)$ is the force on the bottom plate, m_f is the mass of the filament and g is the gravitational acceleration. Eq. (3) does not account for the initial shearing contribution due to the no-slip boundary condition on the plates [14]. The reason for omitting this contribution is that we did not use standard flat plates for this study as discussed in the following section.

2.2.1. Plate design for measuring non-sticky samples

The FSR-technique relies on the sample sticking to the end plates during the stretch experiment. Slip-off is an issue even for the most studied polymer in the FSR, polystyrene (PS). With PS, it is possible to circumvent this problem by increasing the prestretch i.e. increasing the area that sticks to the plate relative to the area of the midfilament plane. Increasing the prestretch was not sufficient in the case of the PE/PO solutions as the presence of PO resulted in greasy samples that slipped off very easily. To overcome slip-off, several new plate geometries were designed. The best design is shown in Fig. 1a and is in the following referred to as the "mushroom plate". The mushroom plate differs from the standard plate (Fig. 1b) in the way that it has an extra plate on top of the standard plate separated by a small rod. The additional plate and rod is referred to as the "mushroom".

The mushroom plate required a special moulding procedure inside the FSR in order to anchor the "mushroom" into the fluid. The moulding procedure is illustrated in Fig. 2. First the sample disc was sandwiched between the two plates and thick tin foil was wrapped around the plates. Second, the sample was heated to

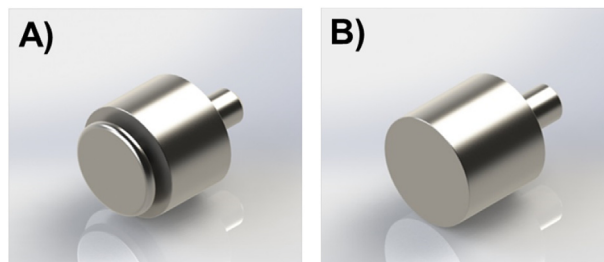


Fig. 1. Sketch of plate designs. (a) The mushroom plate design developed for stretching of non-sticky samples. (b) The original plate design for sticky samples.

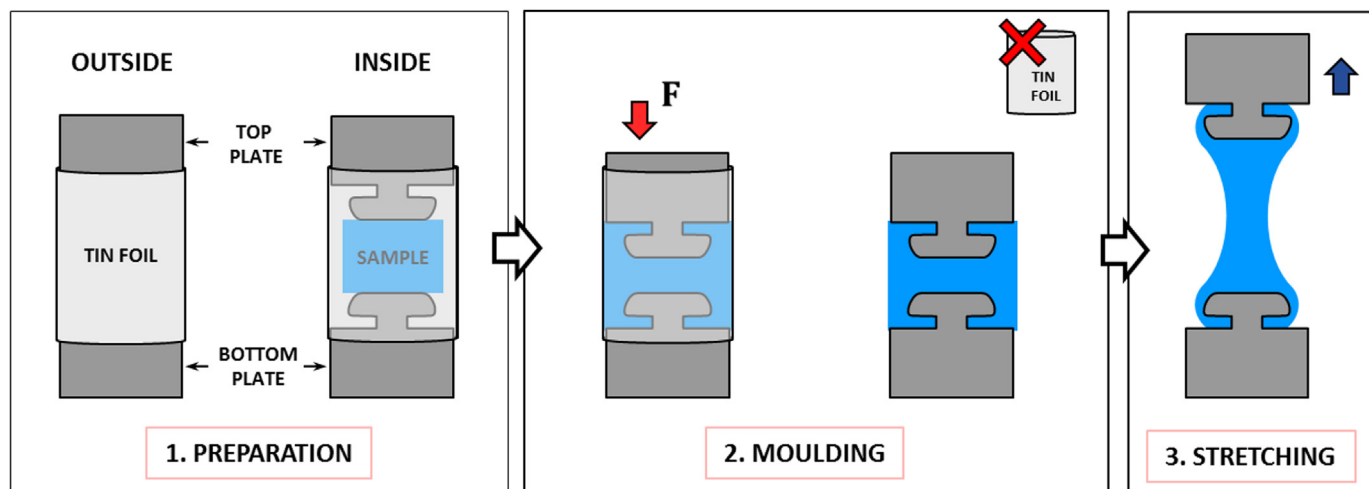


Fig. 2. Sketch of moulding procedure in the FSR using the mushroom plates. 1. Preparation: Initial placement of the polymer disc between the bottom and top plates with a piece of tin foil wrapped around it. 2: Moulding: (left) Moulding procedure where the sample is heated above T_m and the top plate is lowered by applying a force F . (right) after moulding where the tin foil has been removed. 3. Stretching: The anchoring effect of the mushroom during stretching preventing slip-off.

165 °C and the top plate was lowered so that the polymer filled the entire space. As a result, the sample encapsulated the mushroom such that it acted as an anchor upon stretching.

2.2.2. Filament stretching at a constant strain rate with simultaneous high-speed imaging

We conducted experiments at a constant Hencky strain rate $\dot{\epsilon}$ such that throughout the entire experiment the strain increased linearly with time: $\epsilon = \dot{\epsilon}t$. The procedure for each stretch experiment was as follows. After moulding in the FSR as described in the previous section, the sample was heated to 165 °C where it was pre-stretched and relaxed for 15 – 60 min depending on the relaxation times of the sample. The temperature was then changed to the experimental temperature at which the sample was stretched at a constant rate. High-speed imaging of the sample during stretch was performed with a high-speed camera (FASTCAM Mini UX100 from Photron) and a LED light source. Both were placed on the same side of the sample where windows in the oven enabled the stretch to be captured. The frame rate was relatively low (50–1000 fps) and determined by the stretch rate of the given experiment - higher strain rates required higher frame rates.

3. Results and discussion

3.1. Linear rheology

Linear rheology of the three samples along with respective multimode Maxwell model fits are seen in Fig. 3a. The response is given in terms of storage and loss moduli G' and G'' , respectively. The first crossover is captured for PE/PO-9 while for PE/PO-17 and PE/PO-29 the first crossover are estimated by extrapolating G' , G'' to lower frequencies. The inverse value of the estimated first crossover frequency gives an indication of the average relaxation time by reptation τ_d . Due to instrument limitations it was not possible to reach the terminal regime of the samples (the region where G' and G'' reach a slope of 2 and 1, respectively) neither the second crossover found at higher frequencies. For the three samples the average reptation time is between $10^2 - 10^3$ s.

The vertical shift between the samples arise from differences in concentration. That is in accordance with the tube model stating that the plateau modulus G_N^0 scales with ϕ as follows $G_N^0(\phi) \propto \phi^{1+\alpha}$ with the dilution exponent $\alpha = 1$ or 1.3 [15, 16]. The plateau

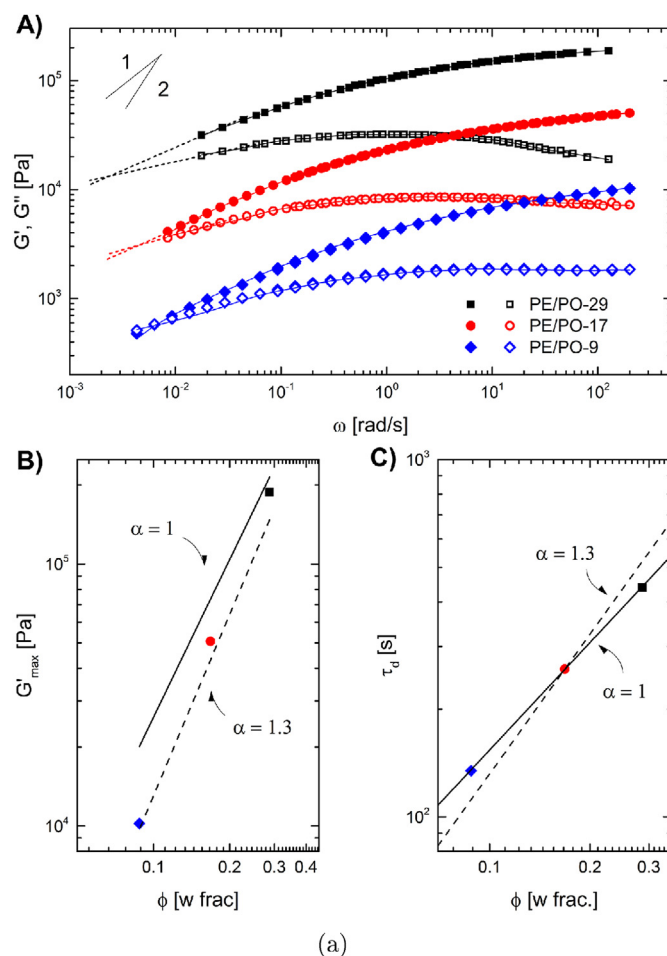


Fig. 3. Linear response of PE/PO solutions at 150 °C. (a) Dynamic frequency sweep expressed in terms of storage modulus G' (closed symbols) and loss modulus G'' (open symbols). Solid lines represent best fit of the multi mode Maxwell model, dashed lines are extrapolations of G' and G'' such that the first crossover can be estimated. (b) Evolution of G'_{\max} with concentration. Solid and dashed lines represent the tube model predicted evolution of G_N^0 with ϕ using $\alpha = 1$ and $\alpha = 1.3$, respectively. (c) Evolution of τ_d with concentration. Solid and dashed lines represent scaling laws of τ_d predicted by the tube model using $\alpha = 1$ and $\alpha = 1.3$, respectively.

modulus is the value observed in G' for a monodisperse well entangled polymeric liquid in the plateau region between the first and second crossover. For undiluted polymers this value is a material constant and for PE at 150 °C the value is $G_N^0 = 2.6$ GPa [17]. The plateau region is not clearly identified in these samples both due to polydispersity and due to the limited range of experimentally accessible frequencies ω . As an approximation for G_N^0 we use G'_{max} which is the value of G' at the highest measured frequency where the smallest slope of G' for all samples is measured. Fig. 3b compares the value of G_N^0 predicted by the tube model with the approximated values using G'_{max} . The approximated values are relatively close to the prediction. For the given concentration range the value of α is expected to be 1. In that case, the approximated values increasingly diverge from the prediction as the concentration decreases. That is expected since G' at lower concentrations show a less pronounced plateau compared to the higher concentrations.

According to the tube model the reptation time of a highly entangled linear polymer melt is given by $\tau_d = \tau_e Z^3$ where τ_e is the relaxation time of one entanglement segment [18]. Moreover, dilution increases the distance between entanglements along the chain, thus increasing τ_e . If the solvent and the polymer are isofrictional, the entanglement relaxation time of a diluted polymer chain scales with $\phi^{-2\alpha}$. Since $Z \propto \phi^\alpha$, the scaling of the reptation time with concentration is $\tau_d \propto \phi^\alpha$. Fig. 3c shows the evolution of τ_d estimated from the first crossover with concentration. Evidently τ_d appears to follow the prediction by the tube model quite nicely using $\alpha = 1$. The fact that the systems obey the tube model suggests that PE and PO are isofrictional at equilibrium which is expected since the repeat units of PE and PO are identical.

Fig. 4 shows the normalized linear response of the three solutions. The normalization is performed in accordance with the tube model. Vertically, the data is normalized by $G_N^0 \phi^{1+\alpha}$ assuming $\alpha = 1$. Horizontally, the data is normalized by the relaxation time of one entanglement τ_e which can be estimated experimentally from the second crossover. As already mentioned, the limited range of accessible frequencies using SAOS, does not allow for the second crossover to be determined experimentally. Instead, we approximate τ_e using previously given scaling laws of dilution derived from the tube model combined with the value $\tau_e = 1.1 \cdot 10^{-8}$ s for undiluted PE.

The data in Fig. 4 have been normalized such that the hypothetical second crossover for the three samples overlap at

$\omega \tau_e / \phi^2 = 1$. Fixing the second crossover of all samples at the same position reveals that the plateau region (the frequency range between the first crossover and the second estimated crossover at $\omega \tau_e / \phi^2 = 1$), stretches over 8 to 10 decades. The large span of the plateau confirms that the samples are highly entangled. The sample of highest concentration (PE/PO-29) shows the widest span of the plateau region, indicating the highest number of entanglements, while the sample of lowest concentration shows the most narrow plateau region (PE/PO-9) indicating the lowest number of entanglements. This trend is in accordance with values given in Table 1. Another way to normalize frequency is by the reptation time $\tau_d \propto \phi$ [15,18]. The insert in Fig. 4 shows the phase angle δ versus $\omega \phi$. Curves for all three samples overlap at low frequencies suggesting that the solutions are well mixed and homogeneous in the linear regime.

3.2. Uniaxial extensional behavior

The extensional stress growth coefficient η_E^+ for samples stretched at 150 °C and 170 °C is shown in Fig. 5a and b, respectively. The extensional response at the two temperatures differs significantly. While most samples at 150 °C show an undershoot followed by strain hardening, most samples at 170 °C simply strain soften.

The observed behavior in Fig. 5a and b is unusual for several reasons. First, the qualitative behavior at the two temperatures is not the same throughout the entire stretch. It means that time temperature superposition principle (TTS) does not apply, which it normally does for homogeneous polymeric liquids [19,20]. Second, while strain softening and stress undershoot is a standard behavior for polymers in shear, it is unusual in extension [21]. Third, none of the stretch experiments reach a steady state extensional viscosity [22,23]. The three identified abnormalities (TTS failure, strain softening and absent steady state) suggests that dynamics other than standard chain dynamics are present. As already mentioned PE/PO systems are known to phase separate upon deformation in shear. Under certain conditions this phase separation induces crystallization as well. The high-speed imaging of the filaments during stretching suggests that in extension both phase separation and crystallization occur and, indeed, cause the observed unusual behavior. Overall we define two fundamentally different scenarios encountered during stretching. Scenario 1: Phase separation and Scenario 2: Flow induced crystallization. All samples undergo

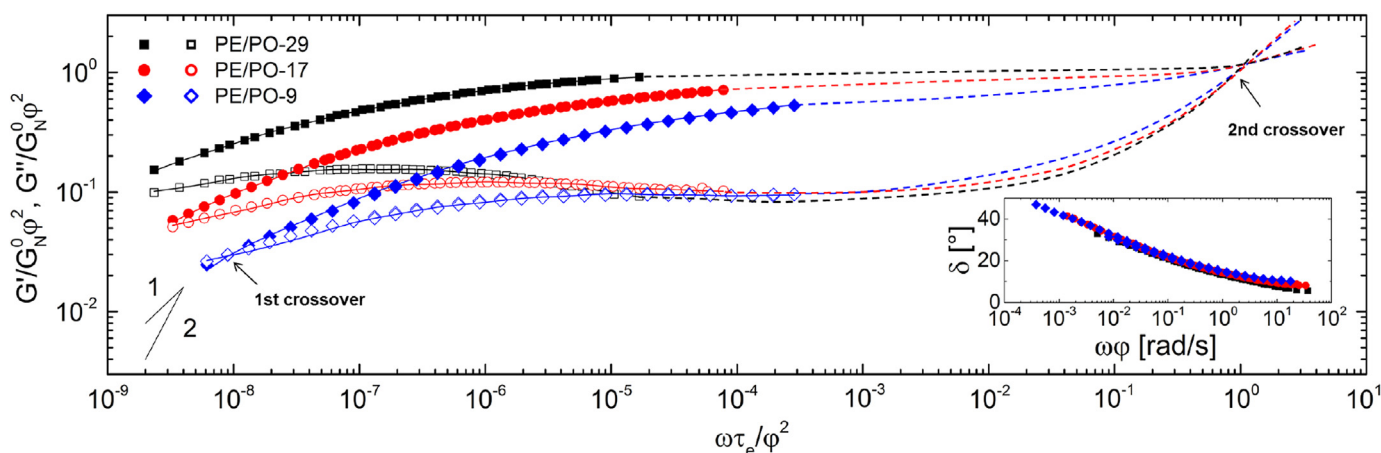


Fig. 4. Nondimensional linear response of PE/PO solutions. Closed symbols represent normalized storage modulus and open symbols represent normalized loss modulus. Solid lines represent best fit of the multi mode Maxwell model and dashed lines are guides to the eye to illustrate the overlap of the second crossover by normalization and thus the extent of the plateau. The insert shows the phase angle versus frequency shifted by concentration.

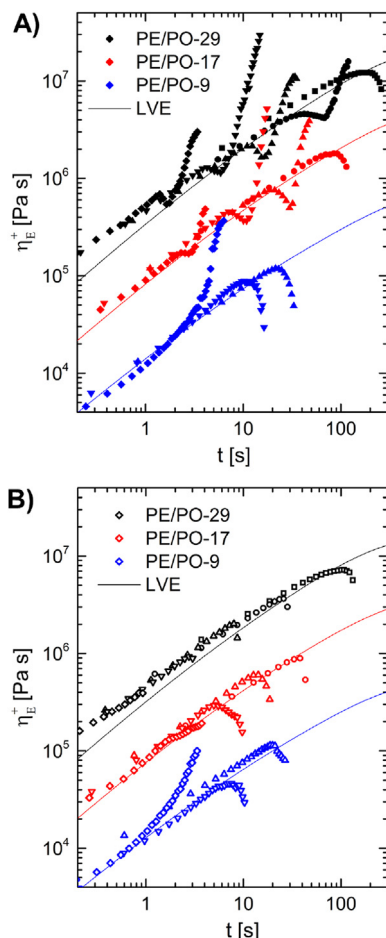


Fig. 5. Nonlinear extensional response of PE/PO-solutions at constant Hencky strain rates. (a) Response at 150 °C, Hencky strain rates (from left to right): PE/PO-29 (Black symbols): $\dot{\epsilon} = 1, 0.3, 0.1, 0.03, 0.01 \text{ s}^{-1}$, PE/PO-17 (Red symbols): $\dot{\epsilon} = 1, 0.3, 0.1, 0.03 \text{ s}^{-1}$, PE/PO-9 (Blue symbols): $\dot{\epsilon} = 1, 0.3, 0.1 \text{ s}^{-1}$. (b) Response at 170 °C, Hencky strain rates (from left to right): PE/PO-29 (Black symbols): $\dot{\epsilon} = 1.4, 0.41, 0.14, 0.041, 0.014 \text{ s}^{-1}$, PE/PO-17 (Red symbols): $\dot{\epsilon} = 1.5, 0.44, 0.15, 0.044 \text{ s}^{-1}$, PE/PO-9 (Blue symbols): $\dot{\epsilon} = 1.5, 0.44, 0.15 \text{ s}^{-1}$. Lines represent the linear viscoelastic envelope obtained from the multimode Maxwell model. (For interpretation of the references to colour in this figure legend, the reader is referred to the Web version of this article.)

either Scenario 1 or 2 during stretching depending on the imposed conditions. Following is a detailed description of the two scenarios.

3.2.1. Scenario 1 - phase separation

Samples stretched at 170 °C appear to phase separate at $\epsilon > 0.9$ causing the observed strain softening of the samples Fig. 5b. Cromer et al. have investigated conditions for amplification of concentration fluctuations in polymer solutions undergoing planar extensional flow [24]. Using a two-fluid model with a Rolie-Poly model for the polymer, they predict growth of concentration fluctuations in steady extensional flow with amplification peaks near $\dot{\epsilon} \sim \tau_d$ and $\dot{\epsilon} \sim \tau_R$ where τ_d and τ_R are the reptation time and the Rouse time for the Rolie-Poly model, respectively. In our experiments we have a broad spectrum of relaxation times with stretch rates within the corresponding range. It is therefore plausible that the same mechanism is responsible for growth of concentration fluctuations in our experiments once a significant orientation of the polymer chains has been established, which is to be expected around a Hencky strain of unity in agreement with our observations for onset of turbidity. We propose that the phase separation and

eventual filament disintegration is the ultimate result of the concentration fluctuation.

The phase separation and thus the course of deformation differs depending on the imposed rate and the concentration of the sample. For samples stretched at 170 °C, the largest difference in behavior is observed between samples of high concentration stretched at low rates (Fig. 6a) and samples of low concentration stretched at high rates (Fig. 6b).

For samples of high concentration, stretched at low rates, the phase separation induces multiple large cracks in the midfilament region (see Fig. 6a), a behavior reminiscent of crazing. Filament failure follows immediately after, disabling Hencky strains $\epsilon > 1.5$ to be reached. As such, the rapid filament failure cannot be considered a brittle fracture [25]. The reason being that the failure is not caused by a single crack propagation, but by multiple cracks propagating simultaneously.

Samples of low concentration, stretched at high rates phase separate as well (see Fig. 6b). As opposed to the above mentioned case, the range of accessible strains as well as the type of filament failure differs.

Phase separation in Fig. 6b is identified as a slight onset of turbidity in the midfilament region at $\epsilon \approx 0.9$. The phase separation propagates at increasing ϵ seen as an increase in turbidity and at $\epsilon > 3$ the phase separation is so pronounced that the surface of the filament becomes uneven and lumpy. Failure of the filament occurs through thinning of the filament during which, phase separation is even more evident.

The stretch experiments presented in Fig. 6a and b show the extremes of Scenario 1. All samples stretched at 170 °C show a behavior somewhere in between the two presented extremes. Fig. 7a shows the gradual transition from one extreme to the other for PE/PO-17 and the following two trends should be noted. 1) With increasing $\dot{\epsilon}$ the degree of strain softening decreases. 2) With increasing $\dot{\epsilon}$ the maximum ϵ that can be reached before failure increases. We hypothesize that both trends are a result of an increased chain stretch for increasing $\dot{\epsilon}$ stabilizing the filament as opposed to the observed phase separation.

3.2.2. Scenario 2 - flow induced crystallization

The strain hardening behavior of solutions stretched at 150 °C, originates from FIC. No samples stretched at 170 °C show signs of FIC.

An example of a stretch in which FIC occurs, is shown in Fig. 8. Analogous to Scenario 1, the sample is still believed to undergo phase separation at $\epsilon \approx 0.9$, due to the observed strain softening behavior combined with the onset of turbidity. At $\epsilon \approx 1.5$ the mid-filament region of the sample transforms from turbid to opaque while the stress starts to rise again. Both observations suggest onset of flow induced crystallization (FIC). An additional indication of FIC is the spontaneous midfilament decrease observed between frames 4 and 5 (indicated by arrows) in Fig. 8. For a fast spontaneous diameter decrease the highly sensitive control scheme of the FSR will counter act the apparent deformation by pushing downward which is indeed the case as observed by the non-monotone motion between frames 4, 5 and 6. Flow induced crystallization can cause such a spontaneous decrease due to the density increase upon crystallization. While this change might seem negligible, it is not. A density increase of $\sim 20\%$ between molten and semicrystalline HDPE would yield a $\sim 7\%$ increase in density for the 29 w% solution of PE in PO. This corresponds to an apparent Hencky strain of 0.06. Given that the decrease in Fig. 8 occurs on the time scale of $\sim 2 \text{ s}$, the FIC contribution to the Hencky strain rate is 0.03 s^{-1} . Relative to the imposed Hencky strain rate of 0.1 s^{-1} , this a significant contribution that does affect the movement of the top plate. Combining all three observations (turbid-opaque transition, density increase and

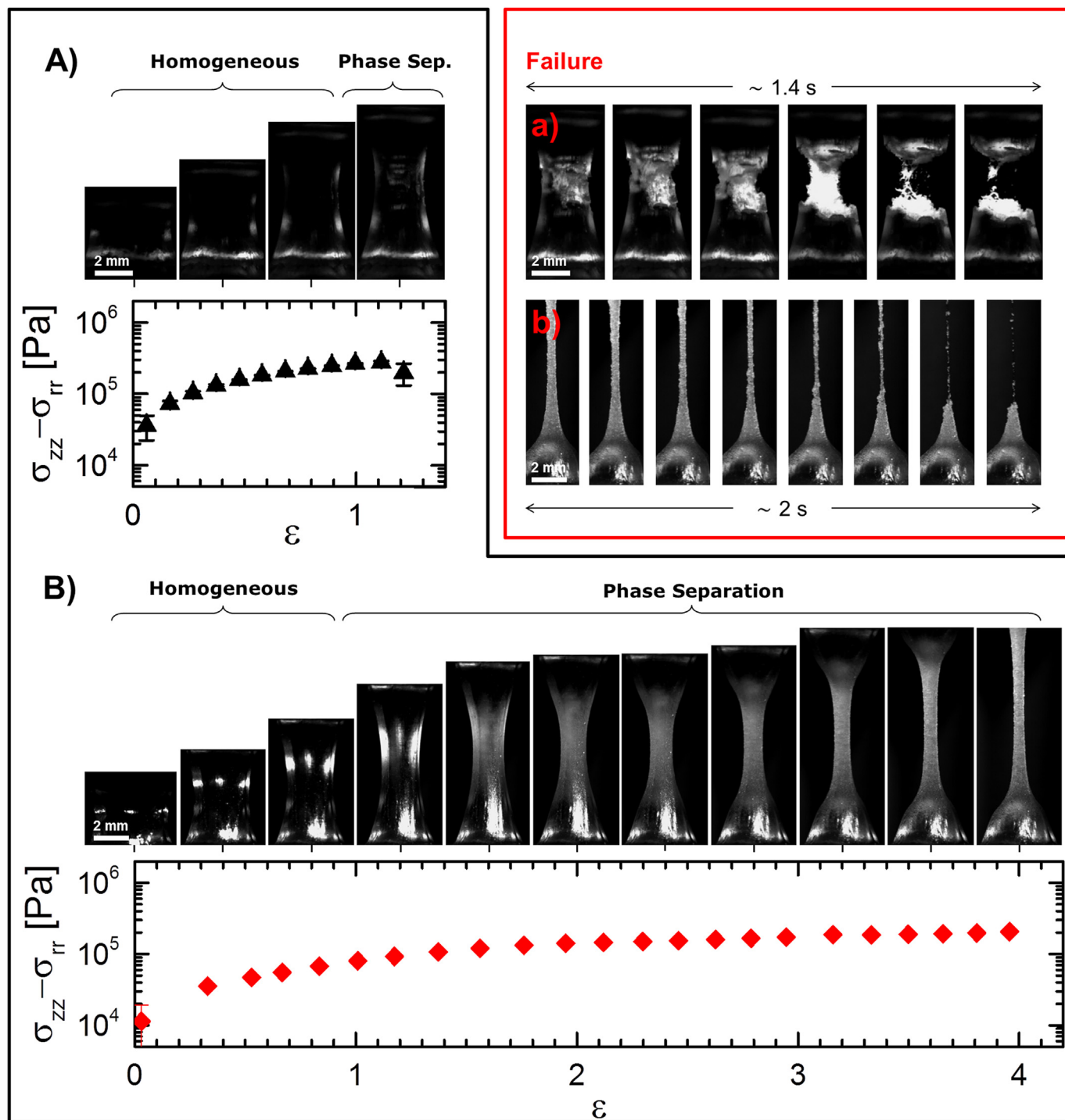


Fig. 6. Examples of rheological response and corresponding images (black frame) as well as failure (red frame) of PE/PO filaments elongated at 170 °C. (a) For a sample of high concentration stretched at low rates. That is PE/PO-29 stretched at $\dot{\epsilon} = 0.014 \text{ s}^{-1}$. (b) For a sample of lower concentration stretched at high rates. That is PE/PO-17 stretched at $\dot{\epsilon} = 1.5 \text{ s}^{-1}$. The bright spots near the edges are due to light source reflections from the filament surface. (For interpretation of the references to colour in this figure legend, the reader is referred to the Web version of this article.)

strain hardening) it is very likely that flow induced crystallization takes place. At $\epsilon > 1.5$ a crystallized neck region develops from the midfilament region causing the significant strain hardening behavior. The transition from molten sample near the plates to the neck area is characterized by an abrupt decrease in diameter along side a sharp transition from transparent to opaque. While the midfilament is deformed the neck area is extended axially by

pulling from the reserve of molten sample at the end plates and into the crystallizing neck. Hence the reserve of molten sample gradually decreases. At $\epsilon > 3$ most of the sample is incorporated into a long crystallized neck. At this point the control scheme starts to fail, not because of an uneven filament, but because the speed of the top plate reaches its maximum speed. Furthermore end plate instability is observed due to the high deformation rates close to

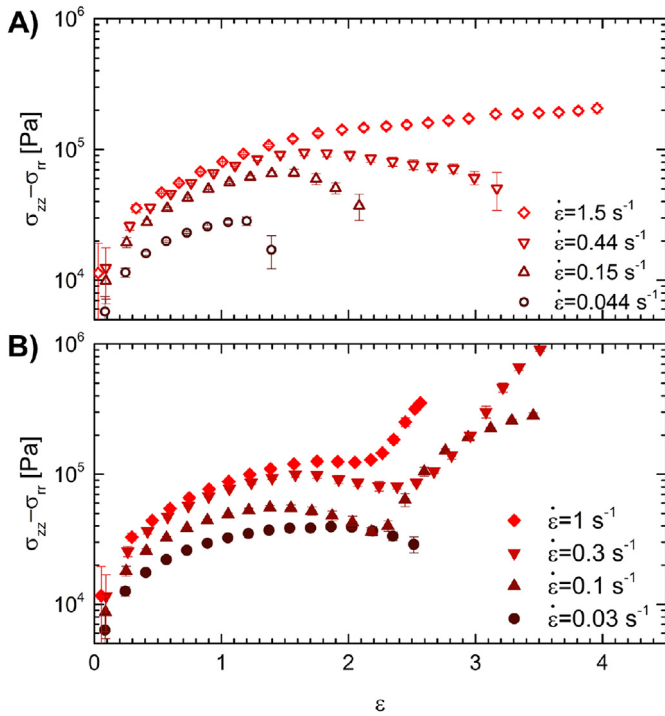


Fig. 7. Extensional stress versus Hencky strain for stretches of PE/PO-17 at a) 170 °C and b) 150 °C.

the plates [26]. At sufficiently high stresses the filament fractures in a brittle manner. DSC measurements of the midfilament region after stretch for a sample stretched under same conditions as in

Fig. 8 showed a rise in T_m of 2.8 °C. The increase in T_m is further proof that FIC has taken place [27].

Fig. 7b shows the stress response of PE/PO-17 at various $\dot{\epsilon}$. The stress undershoot is less pronounced for increasing $\dot{\epsilon}$ suggesting a higher degree of chain stretch, similar to Scenario 1. Samples stretched 150 °C at the lowest rates (i.e. experiments that do not show strain hardening) seem to follow Scenario 1, as well.

3.2.3. Significance of time temperature superposition principle

The high-speed imaging reveals that at small deformations $\epsilon < 0.9$ all samples appear transparent both in Scenario 1 and Scenario 2. The transparency suggests that the samples are homogeneous (i.e. no phase separation or FIC) at strains $\epsilon < 0.9$. To confirm homogeneity, we compare the normalized extensional response measured at 150 °C and 170 °C (see Fig. 9). Here we assume that TTS works also for the nonlinear response. The characteristic time constant used in the normalization is the average Rouse relaxation time $\tau_R = \tau_e Z^2$. As $\tau_e \propto \phi^{-2}$ and $Z^2 \propto \phi^2$ it is evident that τ_R is independent of dilution and thus all samples have the same value of τ_R . We use previously defined values of the undiluted UHMWPE to estimate τ_R for the solutions. At 150 °C we obtain $\tau_R = 0.11$ s and with a shift factor $a_T = 1.47$, we get $\tau_R = 0.075$ s at 170 °C. The normalized stretch rates are given in terms of the Rouse Weissenberg number $Wi_R = \dot{\epsilon}\tau_R$. It weighs the rate of deformation relative to the rate of relaxation of the weight average polymer chain of the sample. Keeping in mind that the sample is highly polydisperse and that τ_R is based on the weight average molar mass, the fractions of higher molar mass in the samples will have much higher τ_R . It is thus possible to observe nonlinear behavior even at $Wi < 1$.

At small strains, the normalized extensional behavior of all samples in Fig. 9 follow the LVE and obey TTS. The fact that the normalized extensional response follows the LVE and obey TTS

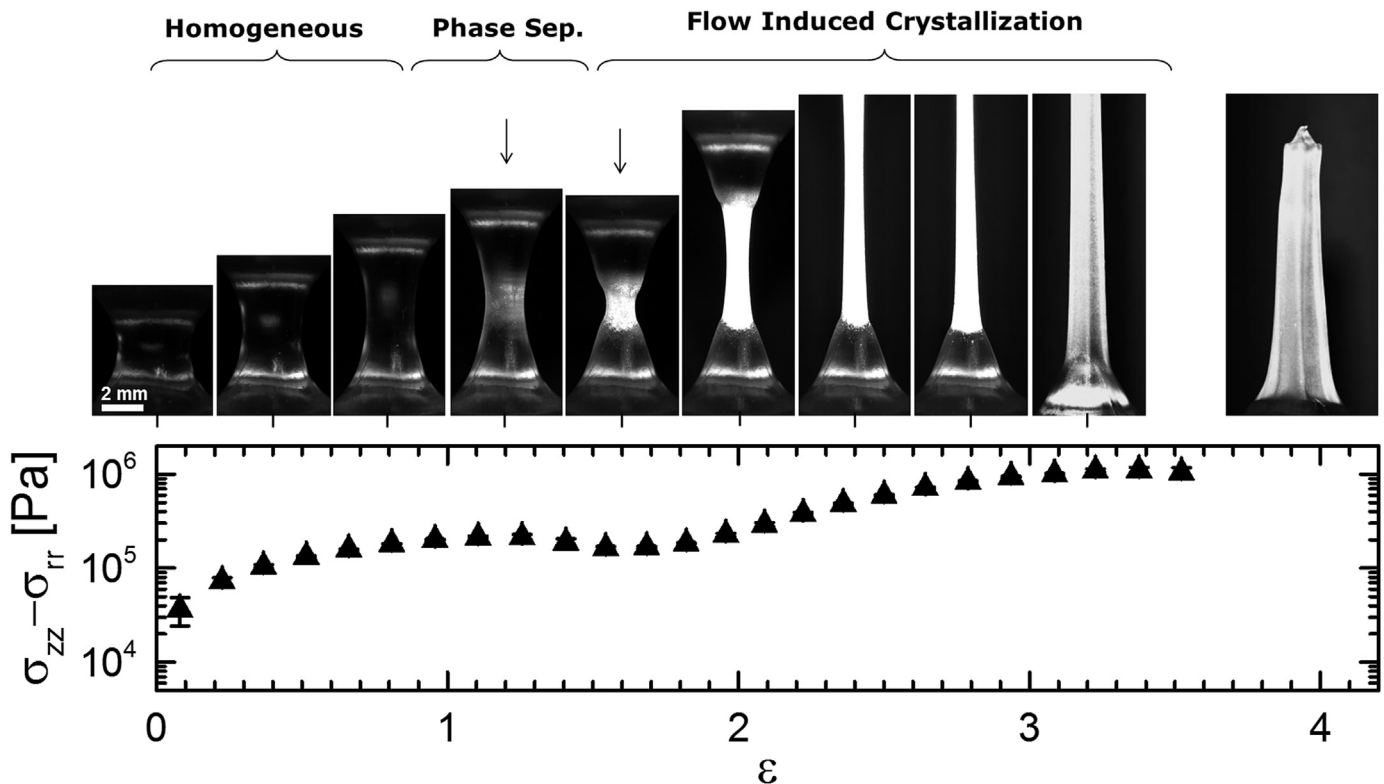


Fig. 8. Example of FIC for stretch experiments performed at 150 °C. The sample is PE/PO-29 stretched at $\dot{\epsilon} = 0.1$ s $^{-1}$. Images are collected through crossed polarizers with light source and camera on the same side. Arrows above image 4 and 5 indicate the strain range in which the onset of FIC occurs. The two images to the far left are taken from a replica of the stretch.

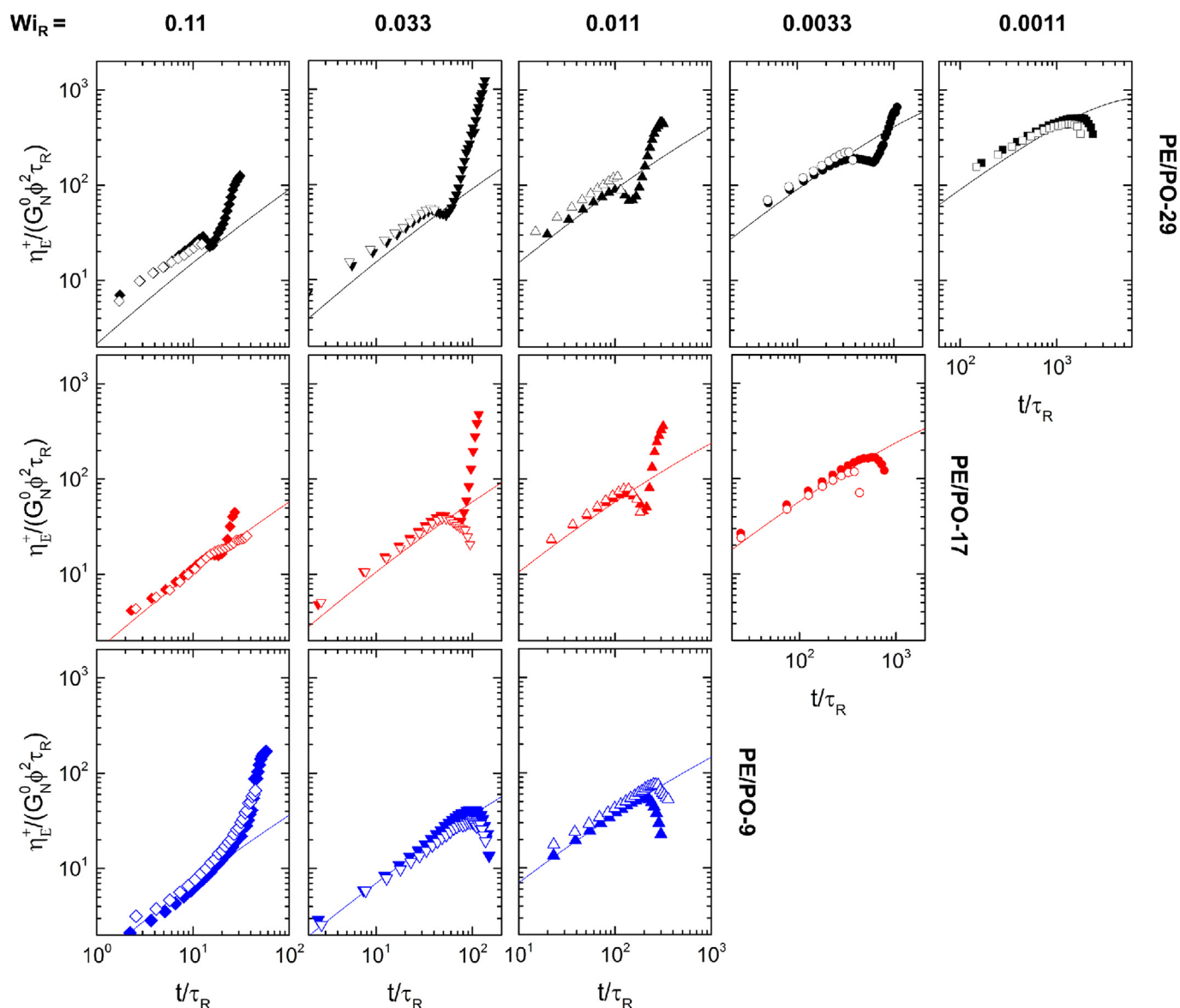


Fig. 9. Normalized nonlinear extensional response at various Weissenberg numbers for PE/PO-29 (top row), PE/PO-17 (middle row) and PE/PO-9 (bottom row). Closed symbols indicate stretches performed at 150 °C. Open symbols indicate stretches performed at 170 °C. Weissenberg numbers apply to both open and closed symbols.

confirms that at small deformations the samples are homogeneous and that the rheology is governed solely by chain dynamics. We observe that in many cases TTS even holds in the strain softening region. This suggests that although the samples are phase separated, the response is still governed by chain dynamics only. However at larger strains the breakdown of TTS confirms that an additional phenomenon (in this case FIC) with a temperature dependency different from that of chain dynamics, occurs. The onset of FIC moves towards earlier times for increasing Wi_R . This is in accordance with general theories stating that the onset of FIC is governed by chain stretch [28].

4. Conclusion

Solutions of UHMwPE in extensional flow show a rich variety of behavior at temperatures well above T_m . We find that at $\varepsilon > 0.9$ the extensional behavior differs fundamentally with concentration, temperature and imposed deformation rate. Overall the observed

behaviors can be divided in two Scenarios 1 - Phase separation and 2 - FIC. At 150 °C flow induced crystallization (Scenario 2) was observed for high Wi_R and high ϕ . The higher the concentration, the lower the Wi_R at which FIC can be detected. E.g. for PE/PO-29, FIC is observed at Wi_R as low as 0.0033, while for PE/PO-9, the lowest Wi_R at which FIC is observed is 0.11. The time at which onset of FIC is observed, decrease for increasing Wi_R . The earlier onset of FIC upon increasing Wi_R is in accordance with the general belief that FIC is governed by chain stretch that increases with Wi_R as well. At lower Wi_R and ϕ the filament only appeared to phase separate (Scenario 1). At 170 °C all samples followed Scenario 1. The observed flow induced phenomena (phase separation and crystallization) are in general agreement with previous studies performed in controlled shear and along a fiber spin-line in which, however, the deformation cannot be controlled. To reach a better understanding controlled extensional rheology in combination with in-situ light scattering or even X-ray scattering will be needed.

Acknowledgement

The authors thank Aage og Johanne Louis-Hansen fonden for financial support as well as Prof. Dimitris Vlassopoulos for fruitful discussions on the work.

Appendix A. Supplementary data

Supplementary data related to this article can be found at <https://doi.org/10.1016/j.polymer.2017.12.042>.

References

- [1] A. Keller, H.W.H. Kolnaar, Materials science and technology, VCH Verlagsgesellschaft mbH (1997) 187–268.
- [2] B.S. Hsiao, L. Yang, R.H. Somani, C.A. Avila-Orta, L. Zhu, Unexpected shish-kebab structure in a sheared polyethylene melt, *Phys. Rev. Lett.* 94 (2005) 117802.
- [3] Y. Ohta, H. Murase, H. Sugiyama, H. Yasuda, Non-newtonian rheological behavior of semi-dilute ultra-high molecular weight polyethylene solution in gel-spinning process. 1: concentration effect on the fundamental rheological properties, *Polym. Eng. Sci.* 40 (2000) 2414–2422.
- [4] H. Murase, T. Kume, T. Hashimoto, Y. Ohta, T. Mizukami, Shear-induced concentration fluctuations in ultrahigh molecular weight polyethylene solutions. 1. Observation above the melting point, *Macromolecules* 28 (1995) 7724–7729.
- [5] H. Murase, T. Kume, T. Hashimoto, Y. Ohta, Shear-induced structures in semidilute solution of ultrahigh molecular weight polyethylene at temperature close to equilibrium dissolution temperature ΔT , *Macromolecules* 38 (2005) 6656–6665.
- [6] H. Murase, T. Kume, T. Hashimoto, Y. Ohta, Time evolution of structures under shear-induced phase separation and crystallization in semidilute solution of ultrahigh molecular weight polyethylene ΔT , *Macromolecules* 38 (2005) 8719–8728.
- [7] H. Murase, Y. Ohta, T. Hashimoto, A new scenario of shish-kebab formation from homogeneous solutions of entangled polymers: visualization of structure evolution along the fiber spinning line, *Macromolecules* 44 (2011) 7335–7350.
- [8] A.J. Pennings, R.J. van der Hooft, A.R. Postema, W. Hoogsteen, G. ten Brinke, High-speed gel-spinning of ultra-high molecular weight polyethylene, *Polym. Bull.* 16 (1986) 167–174.
- [9] A. Pennings, Further studies on the high-speed gel-spinning of ultra-high molecular weight polyethylene, *Polym. Bull.* 23 (1990).
- [10] C. Das, N.J. Inkson, D.J. Read, M. a Kelmanson, T.C.B. McLeish, Computational linear rheology of general branch-on-branch polymers, *J. Rheol.* 50 (2006) 207.
- [11] P. Flory, Principles of Polymer Chemistry, Cornell University Press, 1953.
- [12] J.M. Román Marín, J.K. Huusom, N.J. Alvarez, Q. Huang, H.K. Rasmussen, A. Bach, A.L. Skov, O. Hassager, A control scheme for filament stretching rheometers with application to polymer melts, *J. Non-Newtonian Fluid Mech.* 194 (2013) 14.
- [13] A. Bach, K. Almdal, H.K. Rasmussen, O. Hassager, Elongational viscosity of narrow molar mass distribution polystyrene, *Macromolecules* 36 (2003) 5174.
- [14] H.K. Rasmussen, A.G. Bejenariu, O. Hassager, D. Auhl, Experimental evaluation of the pure configurational stress assumption in the flow dynamics of entangled polymer melts, *J. Rheol.* 54 (2010) 1325.
- [15] Q. Huang, O. Mednova, H.K. Rasmussen, N.J. Alvarez, A.L. Skov, K. Almdal, O. Hassager, Concentrated polymer solutions are different from melts: role of entanglement molecular weight, *Macromolecules* 46 (2013) 5026–5035.
- [16] E. van Ruymbeke, Y. Masubuchi, H. Watanabe, Effective value of the dynamic dilution exponent in bidisperse linear polymers: from 1 to 4/3, *Macromolecules* 45 (2012) 2085–2098.
- [17] L.J. Fetters, D.J. Lohse, R.H. Colby, 2, Ed, in: Physical Properties of Polymers, second ed., Springer, New York, 2007 (Chapter 25), p. 1073.
- [18] M. Doi, Introduction to Polymer Physics, Clarendon Press, 1996, p. 120.
- [19] J. Dealy, D. Plazek, Time-temperature superposition - a users guide, *Rheol. Bull.* 78 (2009) 16.
- [20] M. Kapnistos, A. Hinrichs, D. Vlassopoulos, S.H. Anastasiadis, A. Stammer, B.A. Wolf, Rheology of a lower critical solution temperature binary polymer blend in the homogeneous, phase-separated, and transitional regimes, *Macromolecules* 29 (1996) 7155–7163.
- [21] S. Costanzo, Q. Huang, G. Ianniruberto, G. Marrucci, O. Hassager, D. Vlassopoulos, Shear and Extensional Rheology Of polystyrene melts and solutions with the same number of entanglements, *Macromolecules* 49 (2016) 3925–3935.
- [22] Q. Huang, L. Hengeller, N.J. Alvarez, O. Hassager, Bridging the gap between polymer melts and solutions in extensional rheology, *Macromolecules* 48 (2015) 4158–4163.
- [23] Q. Huang, N.J. Alvarez, Y. Matsumiya, H.K. Rasmussen, H. Watanabe, O. Hassager, Extensional rheology of entangled polystyrene solutions suggests importance of nematic interactions, *ACS Macro Lett.* 2 (2013) 741.
- [24] M. Cromer, M.C. Villet, G.H. Fredrickson, L. Gary Leal, R. Stepanyan, M.J.H. Bulters, Concentration fluctuations in polymer solutions under extensional flow, *J. Rheol.* 57 (2013) 1211–1235.
- [25] Q. Huang, N.J. Alvarez, A. Shabbir, O. Hassager, Multiple cracks propagate simultaneously in polymer liquids in tension, *Phys. Rev. Lett.* 117 (2016) 87801.
- [26] A. Bach, H.K. Rasmussen, P.-Y. Longin, O. Hassager, Growth of non-axisymmetric disturbances of the free surface in the filament stretching rheometer: experiments and simulation, *J. Non-Newtonian Fluid Mech.* 108 (2002) 163.
- [27] B.S. Hsiao, F. Zuo, Y. Mao, C. Schick, Handbook of Polymer Crystallization, John Wiley & Sons, Inc., 2013, pp. 1–30.
- [28] P.C. Roozmond, G.W.M. Peters, Flow-enhanced nucleation of poly(1-butene): model application to short-term and continuous shear and extensional flow, *J. Rheol.* 57 (2013) 1633–1653.